

Experimental Investigation of a High-Efficiency Power Path Controller for a PEM Fuel Cell and Battery Hybrid System

Amirhossein Pahnabi^{1,*}, Hossein Bagherian Farahabadi¹, Mohammad Rezaei Firuzjaei¹,
Reza Youneszadeh¹

¹Northern Research Center for Science & Technology, Malek Ashtar University of Technology, Iran

Article Information

Article History:

Received:

20 Aug 2022

Received in revised form:

16 Oct 2022

Accepted:

05 Nov 2022

Keywords

PEM Fuel Cell

Lead-Acid Battery

Hybridization Circuit

DC/DC Converter

Switch

Abstract

Nowadays, study on alternative sources of fossil fuels for power generation has attracted great attention. Polymer electrolyte membrane fuel cells (PEMFCs) have higher energy densities and lower power densities than conventional batteries. Therefore, PEMFCs should be hybridized with a battery to increase the stability without decreasing the maximum power. Typically, DC-DC converters are utilized to combine these systems leading to a significant increase in cost, size, and weight; moreover, using these converters reduces system efficiency. In this paper, a circuit is implemented into the PEMFC and battery hybridization system with a power path controller. The experimental investigations covers the main challenges in the PEM fuel cell power system implementation, i.e., current ripple and electric power changes dynamics. This circuit implementation increases the system efficiency over 95 percent and decreases the cost by at least 50 percent. The hybridization circuit is verified by simulation and experimental results.

*Corresponding Author: ahpahnabi@mut.ac.ir

Numericulture

Capacitor voltage	U_c
Nernst voltage	E
Absolute temperature (Kelvin)	T
Resistance equivalent of ohmic voltage drop	R_{ohm}
Resistance equivalent of activation voltage drop	R_{act}
Activation voltage drop	U_{act}
Experimental constant	a
Experimental constant	b
Experimental constant	η_0
Capacitor capacity	C
Resistance equivalent of voltage drop caused by concentration	R_{conc}
Fuel cell flow range	I_{limit}
The number of active protons in the power generation process	z
Fuel cell output voltage	U_{out}
Battery open circuit voltage	V_{OCB}
Internal resistance of the battery	R_{Bat}
Battery current	I_{Bat}
Battery charging mode	SOC
Nominal battery capacity	C_{10}
Reference temperature	I_{ref}
Delivery charge by battery	Q
Battery capacity	C_{Bat}
The discharge current is proportional to the nominal capacity	I_{10}
Battery conversion efficiency	η_c
Battery initial charging mode	SOC_0
Battery gas generation voltage	V_g
The final charge voltage of the battery	V_{ec}
Ampere hours stored in the battery	$Ah_{restored}$
Fuel cell flow	I_{FC}
Switch current	I_S
The ratio of dynamic load to total load	α
Switching angular frequency	ω
Load voltage changes	V_L
Changes in the output voltage of the switch	V_S

Internal resistance of the battery	R_b
The normalized value of the battery charge level	s

1. Introduction

The increase in the number of vehicles that use fossil fuel as the only fuel source is the main reason for the pollution of cities. The excessive increase in the use of fossil fuels has caused the worldwide crisis of decreasing oil resources [1,2]. Due to global concerns over dwindling energy sources, pollution, and global warming, fuel cell vehicles (FCVs) have become more popular due to their energy efficiency and low pollution. One way to face this crisis is to use electric cars. These cars use electric power as a drive [3,4]. Increasing the efficiency of electric cars depends on their energy storage system, which is important from two points of view. Firstly, a large amount of energy is stored, and secondly, the system can quickly and accurately respond to the demand of the load (consumer) [5]. Fuel cells (FC) are an effective and reliable source of electricity. Compared with other fuel cells, a polymer fuel cell is the best candidate for use in vehicles due to its high power density and low operating temperature [6]. As a new concept, the fuel cell has been proven to be a prominent power source with little pollution and low operating temperature. However, due to FCs' relative newness, their costs are higher, and many researchers are trying to reduce the costs [7]. Due to advantages such as low pollution, high efficiency, quick start, and low noise, the polymer fuel cell is suitable for use in cars, buses, machines for lifting heavy things, motor boats, and ships [8]. The performance of the polymer fuel cell has been investigated [9]. Another study thoroughly examined the effect of factors such as water flow direction, fuel cell temperature, gas diffusion layer, and the width of the cathode catalyst layer [10].

In the last decade, the study of the use of polymer fuel cells for watercraft has been of great interest and attention. Advantages such as low pollution, low noise, low emission of greenhouse gases and high efficiency have led to various applications of polymer fuel cells in boats and ships [11-18]. One study proposed a real-time control strategy to control the energy distribution in the fuel cell and battery hybrid electric system [11]. They used a closed-loop control system to control the energy system based on DC/DC converters. The first sailboat with a polymer fuel cell propulsion system was developed by MTU Friedrich Schaffen in 2003 [12]. In 2007, the hydrogen-materials group at the University of Birmingham replaced a boat's diesel engines with a polymer fuel cell-battery hybrid propulsion system [13]. In 2012, the Istanbul Technical University of Turkey presented a boat with a fuel cell-battery hybrid power system. The 8 kW fuel cell of this boat is supplied by the Canadian Hydrogenic Company [14]. In line with the Zemship project [15] in Hamburg in 2008, a ship equipped with a fuel cell propulsion system with a capacity of 100 passengers and a maximum speed of 14 kilometers per hour without producing harmful pollution was sent to inland waters. The propulsion system of this ship is designed similar to submarines U212 and U214 [16]. In addition, a polymer fuel cell-lead acid battery hybrid system was also presented for direct power transmission for engine propulsion [17]. In 2009, a boat equipped with a polymer fuel cell system called Nemo H2 was sent to the Amsterdam canals. This boat is equipped with a 60 kilowatts polymer fuel cell and a 70-kWh lead-acid battery pack. The maximum speed of this boat is 16 kilometers per hour. Stack Sazi Nedastak has built two polymer fuel cell modules with a power of 30 kilowatts for this boat. This boat has six tanks with a capacity of 24 kg under a pressure of 350 bar to store hydrogen, which can supply the system with hydrogen for up to 9 hours without recharging [18]. Using the battery and supercapacitor in combination with the fuel cell system increases the performance and ef-

iciency of the fuel cell. The battery can be charged and discharged with a high energy density, and the supercapacitor is mostly used for fast charging and discharging. If the battery is discharged quickly, its internal losses will increase. Therefore, the supercapacitor is mostly used for transient conditions, i.e., starting time and sudden load [19]. In systems with a fuel cell power generation source, a power converter is used to bring the voltage level to the desired voltage level for energy sources [20]. For example, In [21], the optimal design and control strategy of a hybrid fuel cell system with a battery and a supercapacitor have been studied for an electric vehicle. In reference [22], a polymer fuel cell system with a battery has been developed for the propulsion system of a 20-meter long tourist boat. They presented non-linear control of the fuel cell hybrid system with a battery and supercapacitor; however, this is very difficult in terms of practical implementation due to the complexity of the controller [23,24]. Another study discussed the issue of removing the converter from the hybridization system, but the system has a high implementation cost due to its required equipment, and of course, the operational implementation was not carried out to confirm the accuracy of the claimed efficiency [25].

In this study, a polymer fuel cell hybrid system with lead-acid batteries was implemented to provide the required power of a boat engine. The presented system was tested through operational implementation with a 1 kW fuel cell and 12 V and 408 W boat engine load. By removing the DC-DC converter from the hybridization system, the overall system's efficiency increased to 95%. Furthermore, it should be noted that the system cost was reduced by more than 50%. The novelty of the paper is mainly in the experimental investigation of a famous buck converter in the fuel cell boat application. The challenges of the experimental implementation were mainly in the circuit integration with a specific PEM fuel cell, which had some requirements concerning the fuel cell current ripple and power change dynamics.

2. Modeling

2.1. Polymeric Fuel Cell Modeling

The dynamic modeling of the polymer fuel cell is necessary to predict and evaluate its behavior in different conditions. In a fuel cell, the output voltage is lower than the internal voltage due to voltage drops. Ohmic voltage drop, activation voltage drop, and voltage drop caused by concentration are among the most important voltage drops in the polymer fuel cell. Inside the fuel cell, the membrane separates the electrodes, which leads to layers with two opposite poles [26-28]. The equivalent circuit of the fuel cell is shown in Figure 1.

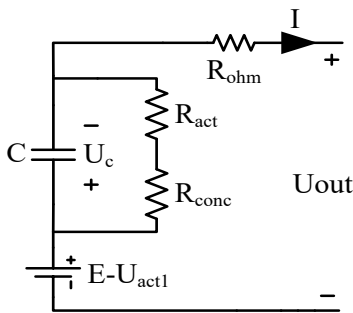


Fig 1. Fuel cell equivalent circuit.

The output voltage of the fuel cell is expressed in the form of equation (1):

$$U_{out} = E - U_{act} - U_c - U_{ohm}$$

$$U_{act1} = \eta_0 + (T - 298).a \quad (1)$$

$$U_c = (I - C \frac{dU_c}{dt}).(R_{act} + R_{conc})$$

The activation voltage drop consists of two parts, as seen in equation (2).

$$U_{act} = U_{act1} + U_{act2} \quad (2)$$

The first part (U_{act1}) is affected by the temperature of the fuel cell and does not depend on the current. The second part (U_{act2}) depends on the current and is modeled by the activation resistance. The resistance equivalent to the activation voltage drop is obtained from equation (3).

$$R_{act} = \frac{U_{act2}}{I} = \frac{T.b.\ln(I)}{I} \quad (3)$$

The resistance corresponding to the concentration drop is obtained from equation (4).

$$R_{conc} = \frac{U_{act2}}{I} = \frac{RT}{zFI} \ln\left(1 - \frac{I}{I_{limit}}\right) \quad (4)$$

2.2. Lead-Acid Battery Modeling

In general, the behavior of a battery is described by its voltage. Three states can be considered for a battery: charging, discharging, and overcharging.

The I_{Bat} current is positive during the charging time and negative during the discharging time. Internal resistance is variable and depends on variables such as capacity, charge and discharge current, and temperature. Many models have been presented to evaluate the batteries' voltage. Most of these models are based on laboratory identification of the intrinsic parameters of the battery. The CIEMAT battery model covers a wide range of lead-acid batteries and requires little factory technical data of parameters for modeling [29]. Three processes are considered in this modeling: discharge, charge, and overcharge. The voltage of the discharge, charge, and overcharge state is calculated from relationships (5), (6), and (7), respectively.

$$V_{Bat} = [2.085 - 0.12(1 - SOC)] - \frac{I_{Bat}}{C_{10}} \left(\frac{4}{1 + I_{Bat}^{1.3}} \right) + \frac{0.27}{SOC^{1.5}} + 0.02(1 - 0.007\Delta T) \quad (5)$$

$$V_{Bat} = [2 - 0.16 SOC] + \frac{I_{Bat}}{C_{10}} \left(\frac{6}{1 + I_{Bat}^{0.86}} + \frac{0.48}{(1 - SOC)^{1.2}} + 0.036 \right) (1 - 0.025 \Delta T) \quad (6)$$

$$V_{Bat} = V_g + (V_{ec} - V_g) \left[1 - \exp\left(\frac{0.95 C_{Bat} - Ah_{restored}}{I_{Bat} \tau} \right) \right] \quad (7)$$

In equation (5), the first term expresses the changes in the open circuit voltage according to the state of charge. The second term models the changes in the battery's internal resistance (the sum of the series resistances caused by various phenomena). In this modeling, it is assumed that in the charging process, the overcharging process starts when the battery capacity reaches 95% of its maximum value. During the charging process, until the battery voltage reaches the gas production voltage ($V_c \leq V_g$), the voltage is evaluated using equation (6), and when the battery voltage exceeds the gas production voltage ($V_c > V_g$), the voltage is evaluated with equation (7).

2.3. Hybridization System

Considering the sensitivity of the fuel cell to sudden changes in current, an intermediate circuit is needed to change the electric power source from the battery to the fuel cell to reduce the rate of changes in fuel cell current. In the presented hybridization circuit, the switching circuit provides the connection between the load and fuel cell by continuously switching on and off and changing the width of the switch pulse. The battery and fuel cell current changes to supply the load current should be according to the curves presented in Figure 2.

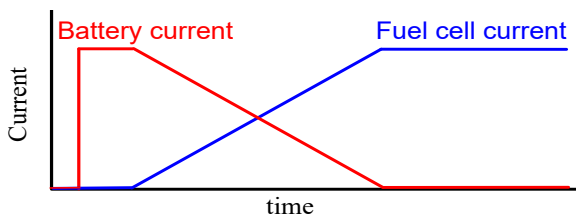


Fig. 2. Battery and fuel cell current changes in providing load current.

The structure of the designed circuit is shown in Figure 3. In this circuit, SW1 (as a current switch) disconnects and connects the fuel cell so that at each step of the switch connection, the current slope may be higher than its tolerable slope. However, over the circuit's whole working time, the fuel flow's average slope becomes less than its maximum tolerable slope. Since the duration of the switch connection is short, there is no damage when the slope of the fuel cell current increases. At first, the battery is connected to the load alone, and until its charging state reaches the desired level, it will not be parallel with the fuel cell. The battery's state of charge cannot be lower than a specific limit because it may be needed in emergency situations. After the battery reaches the desired state of charge, it is paralleled with the fuel cell in such a way that the average power of the load is provided by the fuel cell.

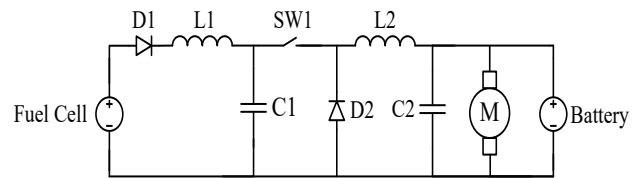


Fig. 3. Hybridization system circuit.

As seen in Figure 3, diode D_1 is used to prevent the current from returning to the fuel cell; diode D_2 plays the role of a snubber diode for inductor L_2 . In this way, when SW_1 is turned off, the current of the L_2 inductor passes through this diode and prevents a sudden increase of voltage on SW_1 , which prevents the switch from burning. When SW_1 is turned off, diode D_2 is connected, which causes a sudden change in its cathode voltage to zero, and as a result, causes current and voltage noise in the head of the fuel cell and the load, respectively. In order to eliminate the effects of switching on the fuel cell and the load, a current low-pass filter for the fuel cell and a voltage low-pass

filter for the load should be used, respectively. In this circuit, the filter on the fuel cell (input) side is used to reduce the current changes caused by the fuel cell switching on. The filter on the load side (output) also reduces the voltage ripple on the load.

2.3.1. Design of Hybrid Circuit Filters

The maximum amount of current changes during switching is 36 amperes, and the amount of instantaneous changes acceptable for a fuel cell is about 0.5 amperes per second. Therefore, to meet the fuel cell’s limitations, the input filter must reduce the current changes up to 98.6 percent in the designed switching frequency. Equation (8) shows the ratio of the fuel cell’s current to the switch’s current, which is extracted from the circuit of Figure 3.

$$\left| \frac{I_{FC}}{I_S} \right| = \left| \frac{1}{\sqrt{(1-L_1C_1\omega^2)^2 + (R_dC_1\omega)^2}} \right| \tag{8}$$

Where, the parameters L_1 , C_1 , and R_d are the size of the inductor and capacitor of the input filter and the dynamic resistance of the fuel cell, respectively. If the current attenuation coefficient of the input filter at the switch frequency is equal to A , then:

$$\left| \frac{I_{FC}}{I_S} \right| < A \tag{9}$$

Using equation (9) and substituting the ratio of currents from equation (8), the boundary conditions for the filter inductor and capacitor can be obtained. This condition is stated in equation (10) and should be considered in choosing the values of L_1 and C_1 .

$$A^2 \left[1 + \omega^2 \left((L_1C_1\omega)^2 + (R_dC_1)^2 \right) - 2L_1C_1 \right] - 1 > 0 \tag{10}$$

As mentioned before, the value of the attenuation coefficient of the filter (A) should be less than X , but is considered equal to X in order to increase the reliability. On the other hand, the internal resistance of the fuel cell (R_d) is 10 mΩ, and the switching frequency is 31 kHz. Therefore, by using these values and solving the inequality of relation (10), a set of suitable solutions for the inductor and capacitor is obtained, see Figure 4. Using Figure 4, the values of $L_1=100\mu\text{H}$ and $C_1=100\mu\text{F}$ for the filter inputs are selected.

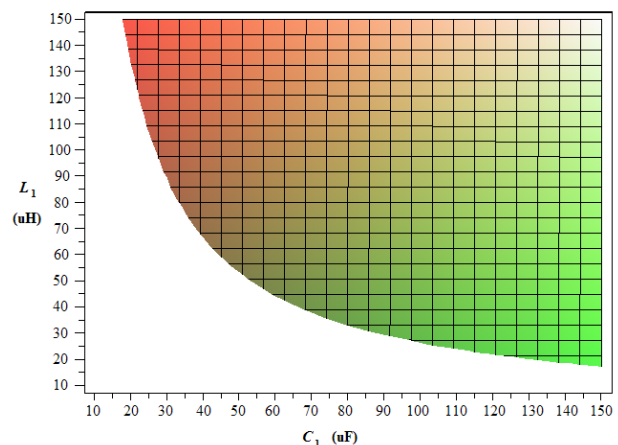


Fig. 4. Set of suitable solutions for inductor and capacitor L_1 and capacitor C_1 .

The purpose of placing the low-pass filter on the load side is to eliminate the voltage ripple on the load. Considering that the filter is checked in AC mode and since the dynamic resistance of the battery is much lower than the load resistance, the load resistance can be omitted. Therefore, equation (11) shows the ratio of load voltage changes to switch output voltage changes.

$$\left| \frac{V_L}{V_S} \right| = \left| \frac{1}{\sqrt{(1-L_2C_2\omega^2)^2 + \left(\frac{L_2}{R_b}\omega\right)^2}} \right| \quad (11)$$

If the attenuation rate of voltage changes is equal to B, then:

$$\left| \frac{V_L}{V_S} \right| < B \quad (12)$$

By simplifying equation (12), a quadratic inequality is obtained, which determines the set of acceptable solutions for inductor L_2 and capacitor C_2 . This inequality is presented in equation (13).

$$B^2 \left[1 + \omega^2 \left((L_2C_2\omega)^2 + \left(\frac{L_2}{R_d}\right)^2 \right) - 2L_2C_2 \right] - 1 > 0 \quad (13)$$

It shows the set of acceptable solutions for inductor L_2 and capacitor C_2 .

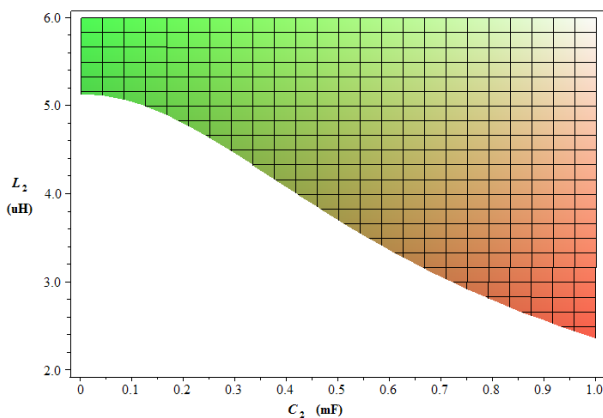


Fig. 5. Set of suitable solutions for inductor and capacitor L_1 and capacitor C_1

Figure 5 shows that if an inductor larger than 5.2 μH is used, the size of the capacitor C_2 can become any value. Therefore, the capacitor C_2 was removed, and the inductor L_2 was selected for 10 μH .

In Figure 3, diode D_1 is used to prevent the return current from entering the fuel cell and protect it. sw_1 controls the power transfer from the fuel cell to the load. In addition, if the fuel cell voltage drops, sw_1 can disconnect it from the battery and the load to increase reliability. Due to the fact that sw_1 is fully connected after a certain period of time, there will be no switching losses in the circuit. The efficiency of hybridization circuit can be calculated as follows:

$$efficiency = \frac{1}{1 + \alpha \left(\frac{1}{\eta} - 1 \right)} \quad (14)$$

The assumed linear relationship between the battery charge, discharge efficiency, and its state of charge can be written as equation (15):

$$\eta = c - rs \quad (15)$$

By placing this relation in relation (14), the efficiency of the hybridization system is obtained as:

$$efficiency = \frac{1}{1 - \alpha \left(1 - \frac{1}{c - rs} \right)} \quad (16)$$

3. Operational Simulation and Implementation

Software simulation in the MATLAB software environment was done to test the performance of the presented hybridization circuit. An element with fast switching capability is needed in the appropriate power, current, and frequency ranges to model the switch in Figure 3. Element IGBT FZ600R12KE3 was used for this purpose. The mentioned IGBT element had a very small drop during the working point in this research. For the proper operation of IGBT, a driver cir-

circuit is needed. The circuit schematic and PCB map of the designed and manufactured IGBT driver are shown in Figures 6 and 7, respectively. An ATMEGA128 microcontroller is used to generate a square wave in this circuit, then this wave is given to the input of the IR2113 driver circuit (which has a small output current), and finally, its output is given to the MOSFET transistors used for the IGBT gate driver.

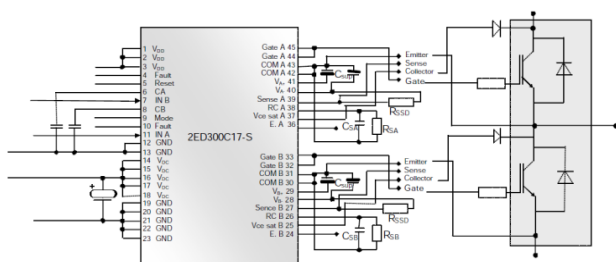


Fig. 6. IGBT driver circuit schematic.

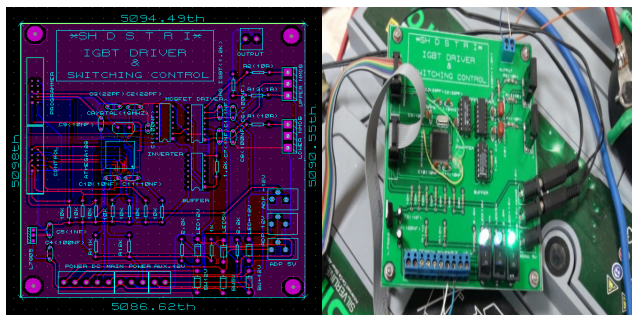


Fig.7. PCB map and IGBT driver hardware implementation.

Diode D_1 must withstand the optimal operating point current of the fuel cell. Also, the diode's



Fig. 10. The boat motor as the system load.

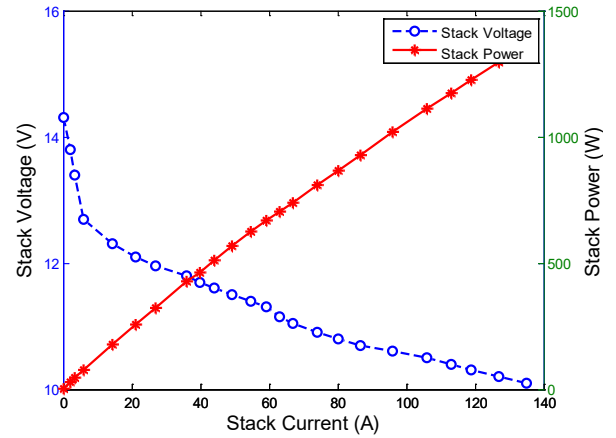


Fig. 12. 1 kW fuel cell polarity diagram

At first, the battery is connected to the load alone, and until its charging state reaches the desired level, it will not be paralleled with the fuel cell. In this case, the efficiency of the designed hybridization system increases. In Figure 11, the overall system efficiency curves for different batteries' state of charge (obtained from the simulation) is shown.

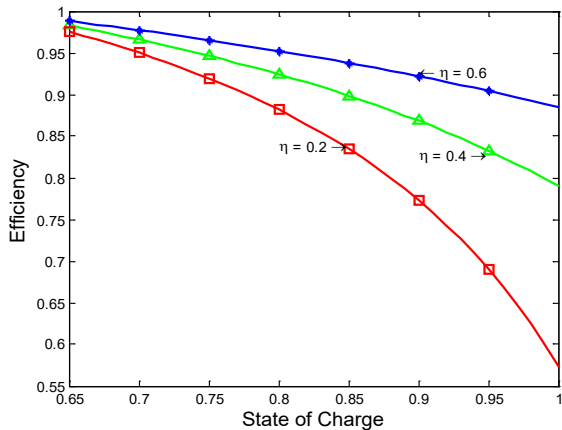


Fig. 11. System efficiency curves according to battery state of charge for different batteries.

As seen in Figure 11, the system's overall efficiency is above 95%. The polarity diagram of the manufactured 1 kW polymer fuel cell is shown in Figure 12.

The results related to the current, voltage, and power of the 1 kW polymer fuel cell resulting from implementation and simulation are shown in Figure 13 to Figure 15, respectively.

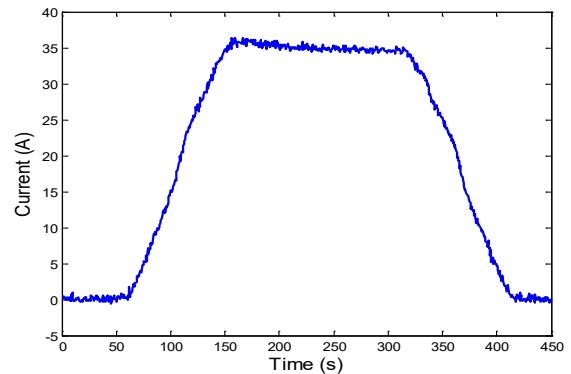


Fig. 13. Flow of 1 kW polymer fuel cell.

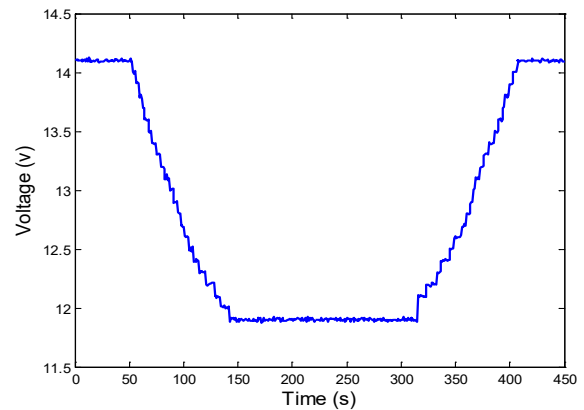


Fig. 14. 1 kW polymer fuel cell voltage.

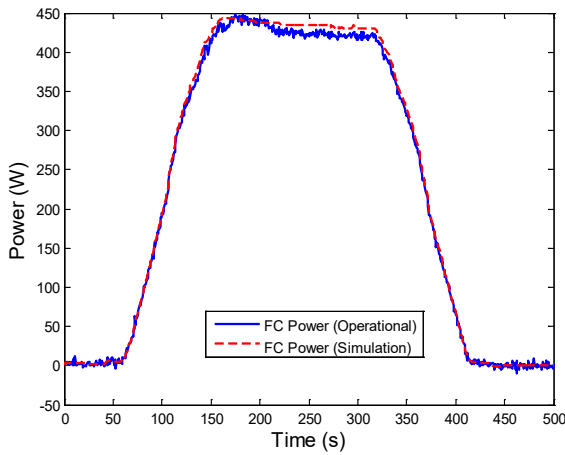


Fig. 15. 1 kW polymer fuel cell power obtained from simulation and operational implementation.

As can be seen, by increasing the current with a suitable slope, the voltage level is reduced, and the fuel cell first reaches its operational working point with a suitable speed and is then fixed with good accuracy. In the same way, the fuel cell output power increases until the current increment stops. By reducing the fuel cell current, the voltage level also increases, and as a result, the output power of the fuel cell decreases in a favorable way. Therefore, according to the obtained results, the system can cope well with the fuel cell power flow switching off and on. The flow diagram of the fuel cell and battery resulting from simulation and operational implementation is shown in Figure 16.

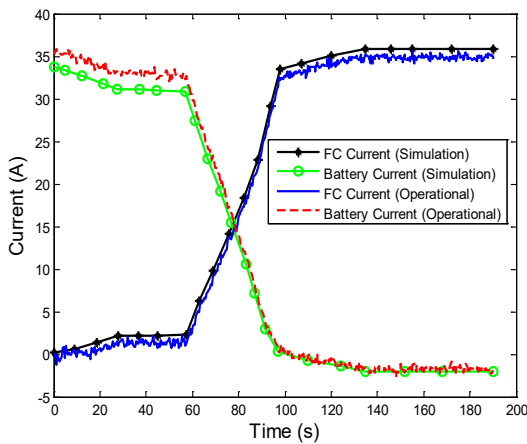


Fig. 16. Fuel cell and battery flow resulting from simulation and operational implementation.

The system efficiency can be measured by measuring the voltage drop from the input to the output of the hybrid system. According to the designed circuit and equipment, the overall system efficiency is more than 95%. The efficiency diagram of the whole system according to the battery charge level obtained from the operational implementation is shown in Figure 17.

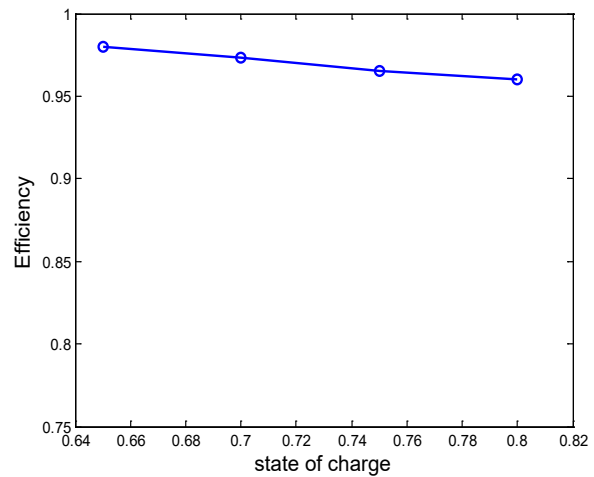


Fig. 17. Overall system efficiency according to battery charge level.

The state of battery charge can not be lower than a specific limit because it may be needed in dynamic conditions. After the battery reaches the desired state of charge, it is paralleled with the fuel cell in such a way that the average power of the load is provided by the fuel cell.

To show the behavior of the hybrid system when the load changes, a state has been considered where the motor speed is initially at 80% of its maximum value and suddenly increases to 100%. Figure 18 shows the operational test results of changing the proposed load.

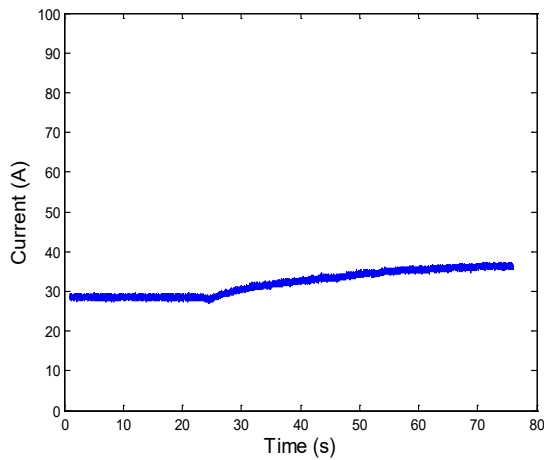


Fig. 18. The load current variation profile (from 80% to 100% of the motor-rated speed).

In the case of a momentary power shock, this dynamic power is provided by the battery because of the battery's lower resistance compared to the fuel cell, preventing probable damage to the fuel cell. Conversely, in case of a load increase in the hybrid system, the fuel cell supplies more current while the battery voltage level decreases.

4. Conclusion

This article presents a circuit for a hybridization system of a 1 kW polymer fuel cell with a lead-acid battery. By implementing the provided electrical circuits, the DC-DC converter has been removed from the hybridization system, which increased efficiency to more than 95% and reduced the hybridization system cost by 50%. The proposed circuit performance was validated by simulations and experimental results. The results proved that the proposed hybridization system has acceptable performance in feeding the load during dynamic and steady state conditions.

Reference

- [1] Song, Y., X. Tan, and S. Mizzi, Optimal parameter extraction of the proton exchange membrane fuel cells based on a new Harris Hawks Optimization algorithm. *Energy Sources, Part A: Recovery, Utilization, and Environmental Effects*, 2020: p. 1-18.
- [2] H. Iqbal, "Electric and hybrid vehicles; design and fundamentals," CRC Press, p. 288, 2003.
- [3] Chang, X., T. Ma, and R. Wu, Impact of urban development on residents' public transportation travel energy consumption in China: An analysis of hydrogen fuel cell vehicles alternatives. *International Journal of Hydrogen Energy*, 2019. 44(30): p. 16015-16027.
- [4] D. Hoelscher, A. Skorcz, Y. Gao, M. Ehsani, "Hybridized electric energy storage systems for hybrid electric vehicles," *IEEE Veh, Power Propuls Conf*, pp. 1-6, 2006.
- [5] S. M. Lukic, R. C. Bansal, F. Rodriguez, A. Emadi, "Energy storage systems for automotive applications," *IEEE Trans Ind Electron*, Vol. 55, pp. 2258-2267, 2008.
- [6] K. Rajashekara, J. Grieve, D. Daggett, "Hybrid fuel cell power in aircraft," *IEEE Ind Appl Mag*, Vol. 14, 2008.
- [7] Duan, J., et al., Research progress on performance of fuel cell system utilized in vehicle. *International Journal of Hydrogen Energy*, 2019. 44(11): p. 5530-5537.
- [8] A. Kheirandish, M. S. Kazemi, M. Dahari, "Dynamic performance assessment of the efficiency of fuel cell-powered bicycle: an experimental approach," *International Journal of Hydrogen Energy*, Vol. 39, pp. 13276-13284, 2016.

- [9] P. J. R. Pinto, T. Sousa, V. R. Fernandes, A. Pinto, C. M. Rangel, "Simulation of a stand-alone residential PEMFC power system borohydride as hydrogen source," *International Journal of Electrical Power & Energy System*, Vol. 49, pp. 57–65, 2013.
- [10] N. Khajeh-Hosseini-Dalasm, M. J. Kermani, D. Ghadiri Moghaddam, J. M. Stockie, "A parametric study of cathode catalyst layer structural parameters on the performance of a PEM fuel cell," *International Journal of Hydrogen Energy*, Vol. 35, pp. 2417–2427, 2010.
- [11] A. Al Amerl, I. Oukkacha, MB. Camara, B. Dakyo, "Real-Time Control Strategy of Fuel Cell and Battery System for Electric Hybrid Boat Application," *Sustainability*, 13(16), p.8693, 2021.
- [12] "First yacht with certified fuel cell propulsion," *Fuel Cells Bull*, Vol. 12, pp. 4-5, 2003.
- [13] "Hydrogen hybrid canal boat," *Green Car Congress*, 2007.
- [14] M. S. Yazici, M. Hatipoglu, "Hydrogen and fuel cell demonstration in Turkey," *Energy Procedia*, Vol. 29, pp. 683-689, 2012.
- [15] M. Limbrunner, "Fuel cell system for zero emission ships: safety concept and experience from operation," *Hannover Messe technical forum*, Hannover, Germany, pp. 4-8, 2011.
- [16] W. Winkler, "Applications transportation: ships: fuel cells," *Elsevier, Encyclopedia of electrochemical power sources*, vol. 1, pp. 338-358, 2009.
- [17] A. Psoma, G. Sattler, "Fuel cell systems for submarines: from the first idea to serial production," *Journal of Power Sources*, Vol. 106, pp. 381-383, 2002.
- [18] F. Vogler, G. Wursig, "New developments for maritime fuel cell systems," *18th world hydrogen energy conference*, pp. 16-21, 2010.
- [19] J. T. Pukrushpan, H. Peng, A. G. Stefanopoulou, "Control-oriented modeling and analysis for automotive fuel cell systems," *J Dyn Syst Meas Control*, Vol. 126, 2004.
- [20] P. Garcia, J. P. Torreglosa, L. M. Fernandez, F. Jurado, "Control strategies for high-power electric vehicles powered by hydrogen fuel cell, battery and supercapacitor," *Expert System Application*, Vol. 40, pp. 4791-4804, 2013.
- [21] O. Erdinc, B. Vural, M. Uzunoglu, "A wavelet-fuzzy logic based energy management strategy for a fuel cell/battery/ultracapacitor hybrid vehicular power system," *Journal of Power Sources*, Vol. 194, pp. 369-380, 2009.
- [22] C. H. Choi, et al, "Development and demonstration of PEM fuel-cell-battery hybrid system for propulsion of tourist boat," *International Journal of Hydrogen Energy*, Vol. 41, n. 5, pp. 3591-3599, 2016.
- [23] M. Rajabzadeh, S. M. T. Bathaee, M. A. Golkar, "Dynamic modeling and nonlinear control of fuel cell vehicles with different hybrid power sources," *International Journal of Hydrogen Energy*, Vol. 41, n. 4, pp. 3185-3198, 2016.
- [24] O. Alavi, et al., "Non-Isolated DC-DC Converters in Fuel Cell Applications: Thermal Analysis and Reliability Comparison," *Applied Sciences*, 2022, 12.10: 5026.
- [25] S. Howroyd, R. Chen, "Powerpath controller for fuel cell & battery hybridization," *International Journal of Hydrogen Energy*, Vol. 41, n. 7, pp. 4229-4238, 2016.
- [26] M. H. Nehrir, C. Wang, "Modeling and control of fuel cells: distributed generation applications," *John Wiley & Sons, Inc*, 2009.
- [27] N. Achaibou, M. Haddadi, A. Malek, "Modeling of lead acid batteries in PV systems," *Energy Pro-*

cedia, Vol.18, pp. 538-544, 2012.

[28] B. Zhang, et al., "Modeling and Decentralized Predictive Control of Ejector Circulation-Based PEM Fuel Cell Anode System for Vehicular Application," *Automotive Innovation*. 2022 Aug;5(3):333-45.

[29] J. B. Copetti, E. Lorenzo, F. Chenlo, "A general battery model for PV system simulation," *Progress in Photovoltaic Research and Application*, Vol. 1, pp. 283-292, 1993.